Supporting Information

Anchoring defective metal-free catalysts on montmorillonite nanosheets for tetracycline removal: synergetic adsorption-catalysis and mechanism insight

Min Li[a], Xudong Liu[a,b], Zhinan Xie [a], Chunfang Du[a*], Yiguo Su[a*]

Inner Mongolia Key Laboratory of Chemistry and Physics of Rare Earth Materials, School of Chemistry and Chemical Engineering, Inner Mongolia University, Hohhot, Inner Mongolia 010021, PR China

Department of Chemistry, Baotou Teachers' College, Baotou, Inner Mongolia 014030, PR China

Corresponding author E–mail: cesyg@imu.edu.cn; cedchf@imu.edu.cn; Fax: +86–471–4994375; Tel: +86–471–4994375

Table S1. Elemental analysis results for C_3N_5 and 10CN-MMT.

Elemental analysis result			
Sample	**N%**	**C%**	**H%**
C_3N_5	**59.8**	**36.5**	**1.77**
10CN-MMT	**0.427**	**0.497**	**0.833**

Table S2. Kinetic parameters of various models.

Kinetic Models	Parameters	C_3N_5	MMT Ns	10CN-MMT
Pseudo–first–order	q_e (mg·g^{-1})	5.69	14.3	38.0
	k_1 (min^{-1})	0.0291	0.0781	0.0870
	R^2	0.930	0.903	0.971
Pseudo–second–order	q_e (mg·g^{-1})	7.93	16.9	44.8
	k_2 (mg·g^{-1}·h^{-1})	0.00201	0.00601	0.00201
	R^2	0.940	0.935	0.988
Webber-Morris	C (mg·g^{-1})	-0.0750	1.34	4.12
	k_{id}	0.609	1.89	5.03
	R^2	0.954	0.927	0.936
Elovich	α	0.226	3.68	12.1
	β	0.399	0.281	0.111
	R^2	0.948	0.955	0.995

Table S3. Isothermal model parameters of TC adsorption over 10CN-MMT.

Models	Parameters			
Freundlich model	$1 \cdot n^{-1}$	k_F ($L \cdot mg^{-1}$)	R^2	Standard error
	2.96	11.8	0.897	2.58
Langmuir model	q_m ($mg \cdot g^{-1}$)	k_L ($L \cdot mg^{-1}$)	R^2	Standard error
	45.9	0.143	0.997	0.01
Redlich-Peterson model	α	K_p ($L \cdot mg^{-1}$)	R^2	Standard error
	0.143	6.56	0.997	0.320
Temkin model	A	K_T ($L \cdot mg^{-1}$)	R^2	Standard error
	10.0	1.39	0.972	0.980

Table S4. The comparison on the catalytic activity of 10CN/MMT activated PMS for pollutant degradation with metal-free catalysts reported in the literature.

Sample	Type of pollutant	C_{pol} (mg·L^{-1})	Reaction time (min)	Degradation efficiency (%)	TOC (%)	Ref.
10CN-MMT	TC	50	120	95.0	81.1	this work
$NBC_{2.0}$	SMX	30	5	99.8	81.7	[1]
***N*-CPANI**	DOX	20	120	91.7	83.8	[2]
BNC	Phenol	30	100	99.6	68.3	[3]
BC-300	Phenol	10	98.3	98.0	46.0	[4]
PWC	BG	10	120	95.0	61.0	[5]
FAC	PFOA	4	360	93.5	84.5	[6]
1NSDMC-30	4-CP	80	60	100	74.1	[7]
PDA-gCN-1.0	SMX	10	5	100	56.1	[8]
CN-CGs	BPA	50	30	90.0	80.0	[9]
SBC	TCS	9.8	240	98.9	32.5	[10]

Table S5. Possible intermediates of TC degradation.

No.	Molecular weight (m/z)	Tentative structure	Detected
–	445	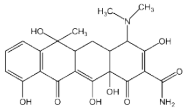	√
P1	428	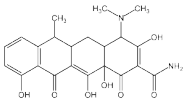	√
P2	362	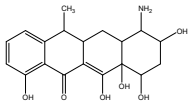	√
P3	318	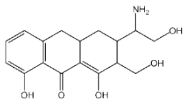	√
P4	415	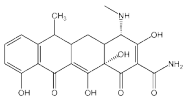	√
P5	400	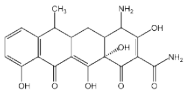	√
P6	318	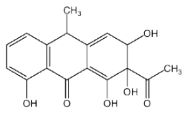	√
P7	274	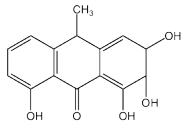	√
P8	460	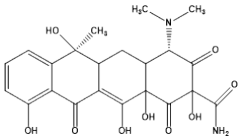	√
P9	218	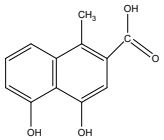	√
P10	174	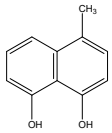	√

P11	122	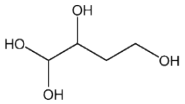	√
P12	100	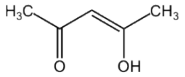	√
P13	83	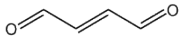	√
P14	61	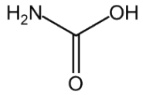	√
P15	130	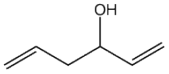	√

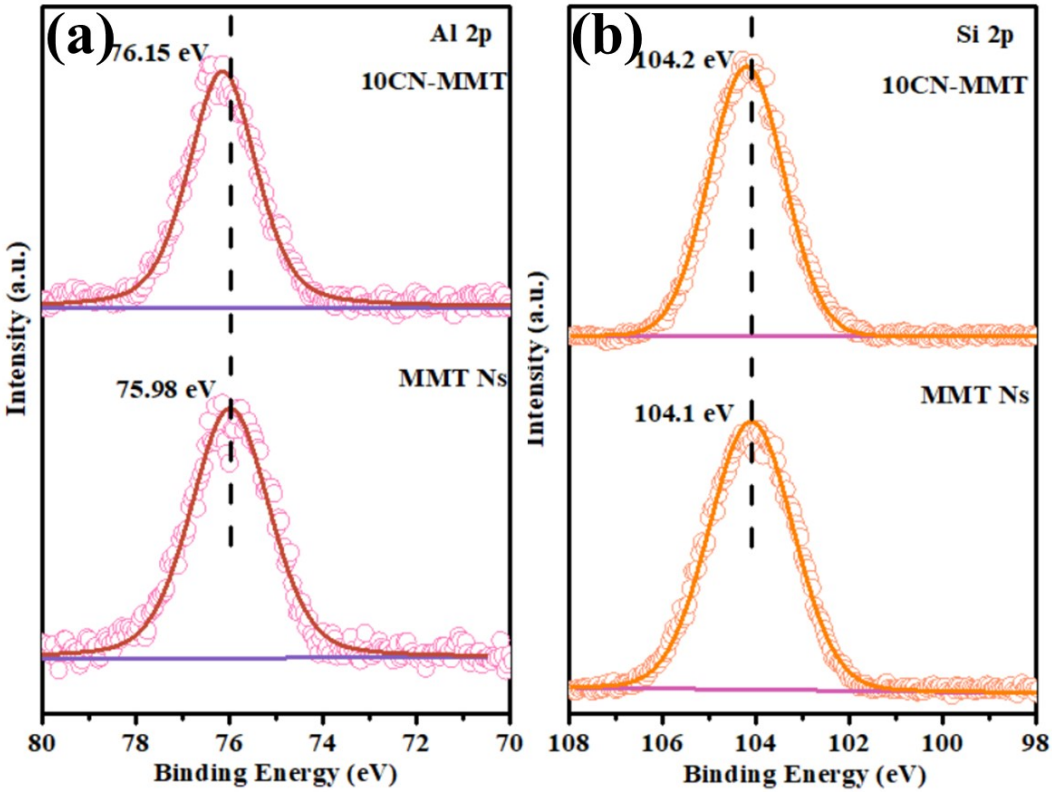

Fig. S1. XPS spectra of Al 2p (a) and Si 2p (b) for MMT Ns and 10CN-MMT.

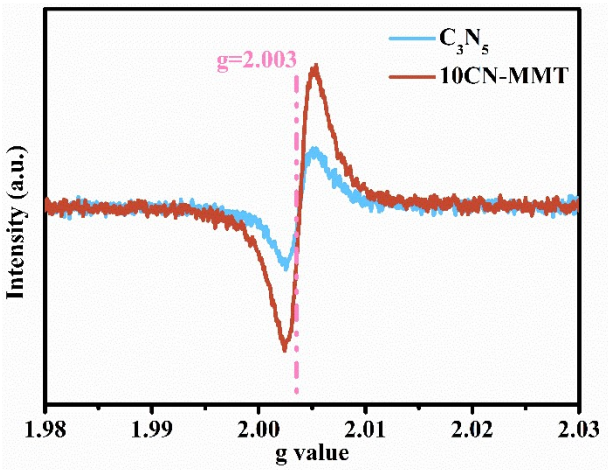

Fig. S2. ESR spectra of C_3N_5 and 10CN-MMT samples at room temperature.

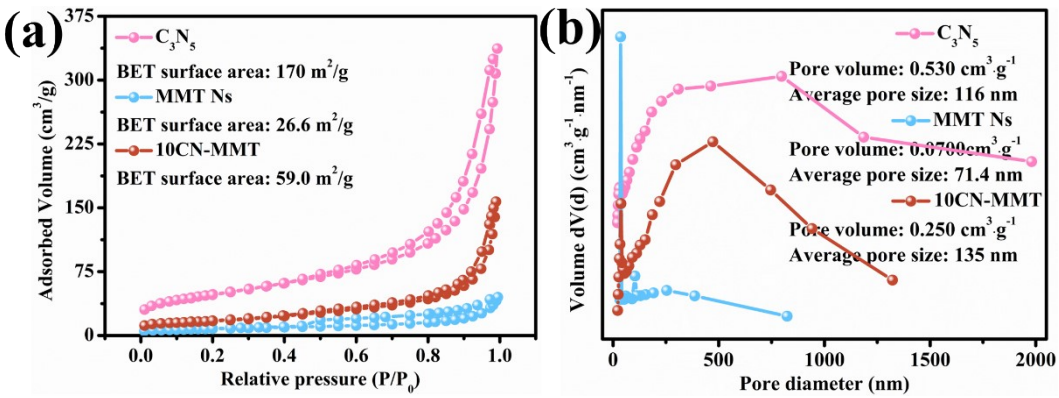

Fig. S3. N_2 adsorption-desorption isotherms (a) and pore size distribution curves (b) of C_3N_5, MMT Ns and 10CN-MMT.

Fig. S3a showed the N_2 adsorption-desorption curves of C_3N_5, MMT Ns, and 10CN-MMT. The N_2 adsorption occurred in the range of relative pressure from 0.5 to 1.0, which indicated that type IV isotherms existed in C_3N_5, MMT Ns, and 10CN-MMT [11,12]. The specific surface area of C_3N_5 could reach 170 $m^2 \cdot g^{-1}$ with pore volume of 0.530 $cm^3 \cdot g^{-1}$ as shown in Fig. S3b. The specific surface area of MMT Ns was small (26.6 $m^2 \cdot g^{-1}$) and concentrated in the range of 2–10 nm, which belonged to the mesoporous structure. 10CN-MMT sample with BET surface area of 58.95 $m^2 \cdot g^{-1}$ was higher than that of pristine MMT Ns. As shown in the TEM image in Fig. 4c, C_3N_5 was highly dispersed on the MMT Ns, and the average pore size (135 nm) of 10CN-MMT was significantly increased compared with MMT Ns and C_3N_5, and the larger and open pore channels were favorable for the adsorption and desorption of PMS and TC molecules.

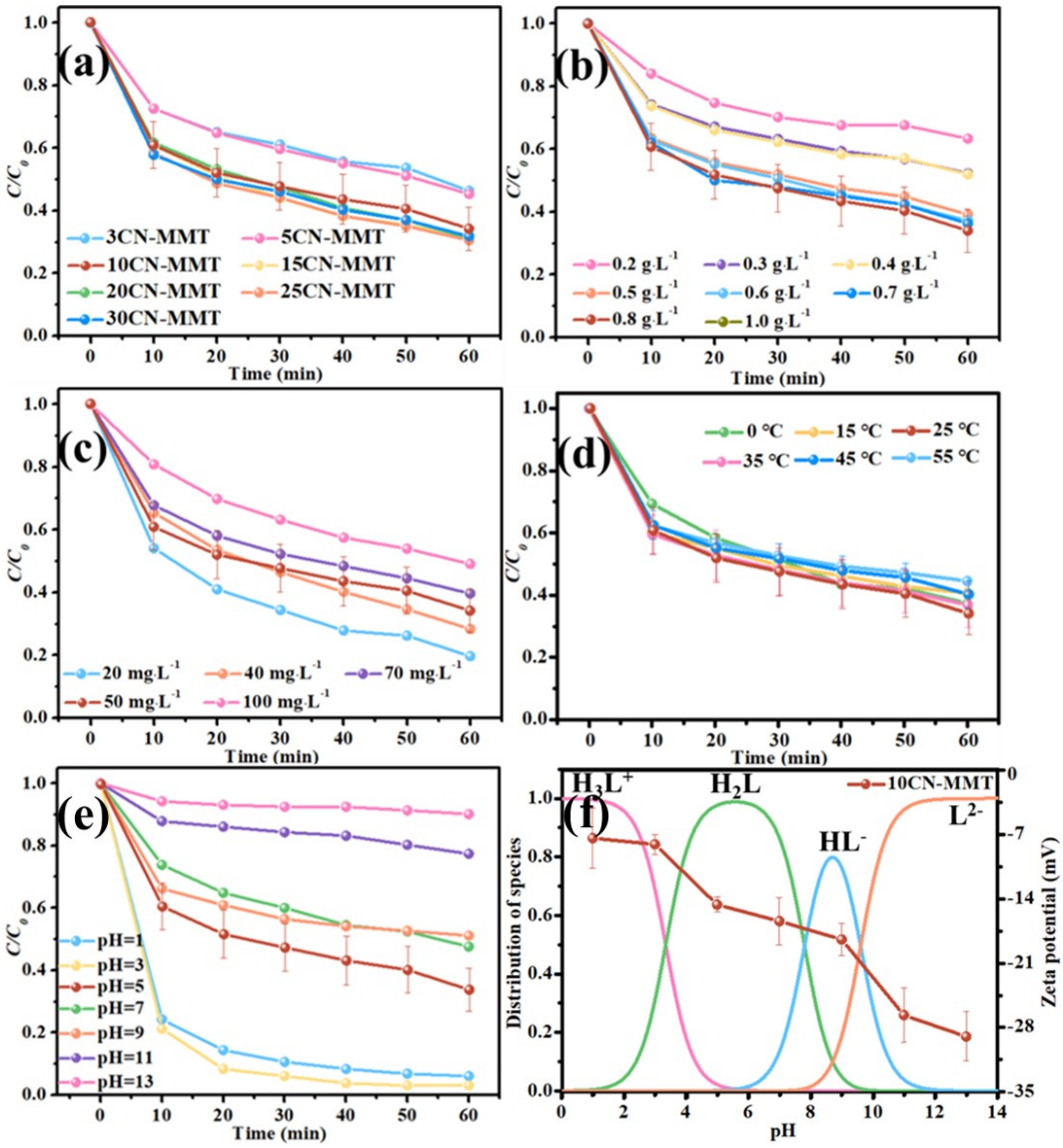

Fig. S4. Effects of CN loading amount (a), catalyst dosage (b), initial TC concentration (c), temperature (d), and pH value (e) on the TC adsorption efficiency. Chemical structure of TC and Zeta potential of 10CN-MMT under different pH values (f). General experiment parameters: [TC] =50 mg· L^{-1}; [10CN-MMT] = 0.8 g· L^{-1}; initial pH = 5.0; T =25 °C.

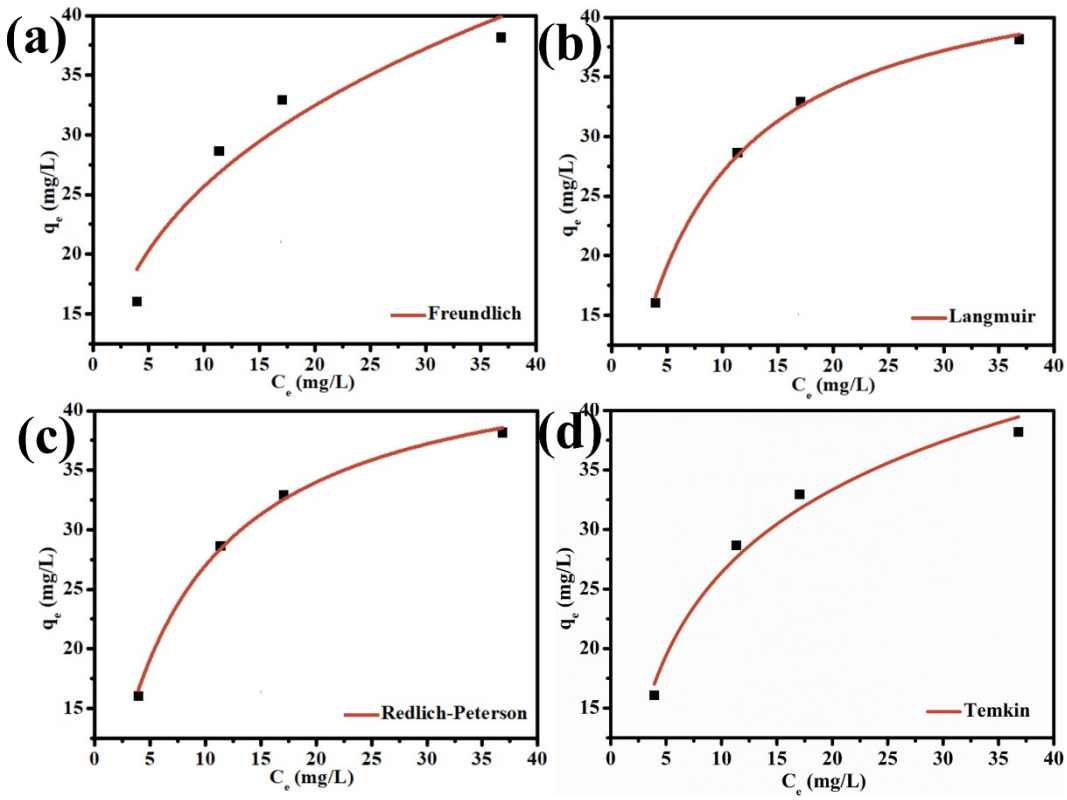

Fig. S5. Freundlich (a), Langmuir (b), Redlich-Peterson (c), and Temkin (d) isothermal models for 10CN-MMT toward TC.

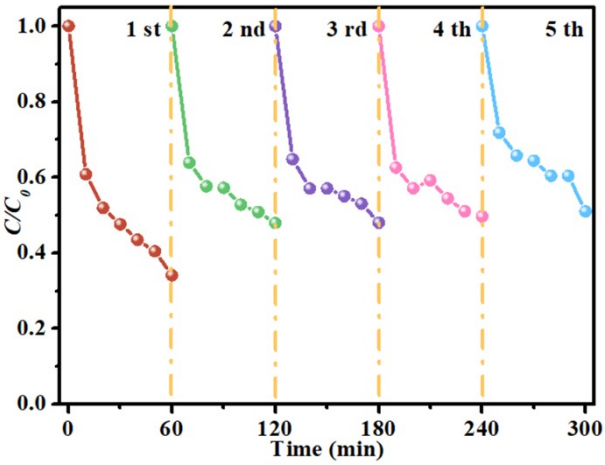

Fig. S6. The cycle performance of TC adsorption over 10CN-MMT.

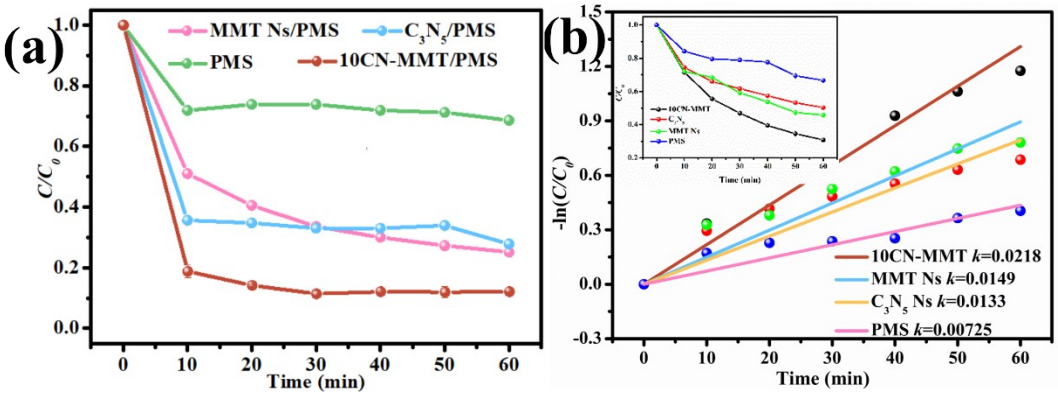

Fig. S7. The degradation performance of various samples toward TC(a). General experiment parameters: [TC] = 50 mg· L^{-1}; [catalyst] = 0.8 g· L^{-1}; [PMS] = 0.3 mmol· L^{-1}; initial pH = 5.0; T = 25 °C. The pseudo first-order kinetic models for various samples toward TC within 60 min (b). General experiment parameters: [TC] = 50 mg· L^{-1}; [catalyst] = 0.4 g· L^{-1}; [PMS] = 0.3 mmol· L^{-1}; initial pH = 5.0; T = 25 °C.

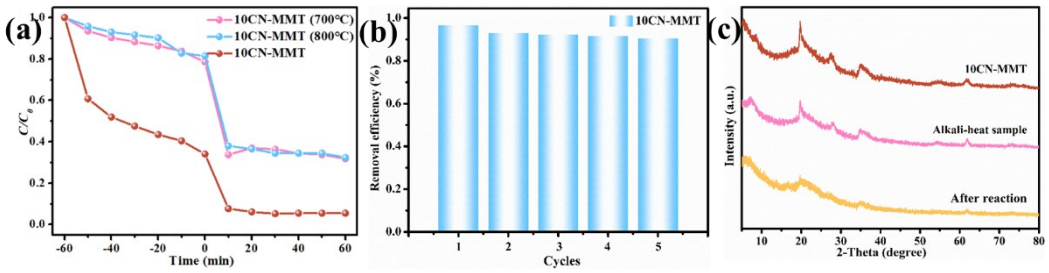

Fig. S8. TC degradation efficiency over 10CN-MMT, 10CN-MMT (700 °C), and 10CN-MMT (800 °C) (a). Recycle tests of TC degradation over 10CN-MMT (b). XRD patterns of 10CN-MMT, alkali-heat sample and the sample after catalytic reaction (c). General experiment parameters: [TC] = 50 mg· L^{-1}; [10CN-MMT] = 0.8 g· L^{-1}; [PMS] = 0.3 mmol· L^{-1}; initial pH = 5.0; T = 25 °C.

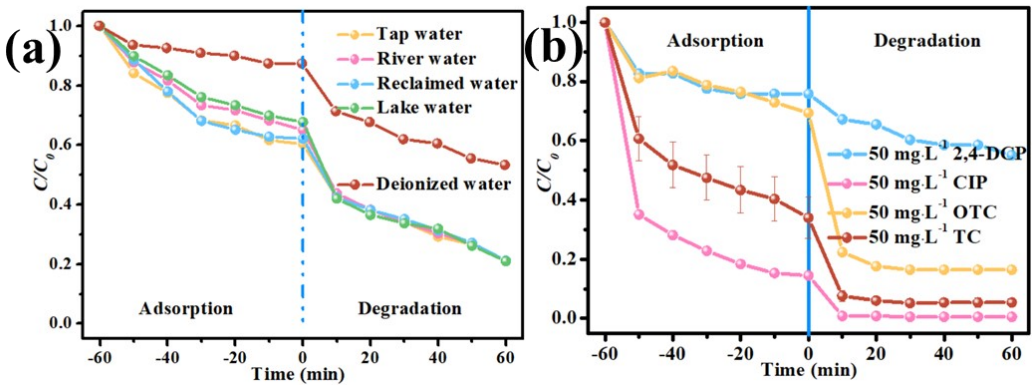

Fig. S9. Degradation efficiencies of TC in different water environments (a). General experiment parameters: [TC] = 50 mg· L^{-1}; [10CN-MMT] = 0.1 g· L^{-1}; [PMS]= 0.3 mmol· L^{-1}; T = 25 °C. The catalytic efficiency of 10CN-MMT toward various organic pollutants (b). General experiment parameters: [TC] = 50 mg· L^{-1}; [10CN-MMT] = 0.8 g· L^{-1}; [PMS] = 0.3 mmol· L^{-1}; T = 25 °C.

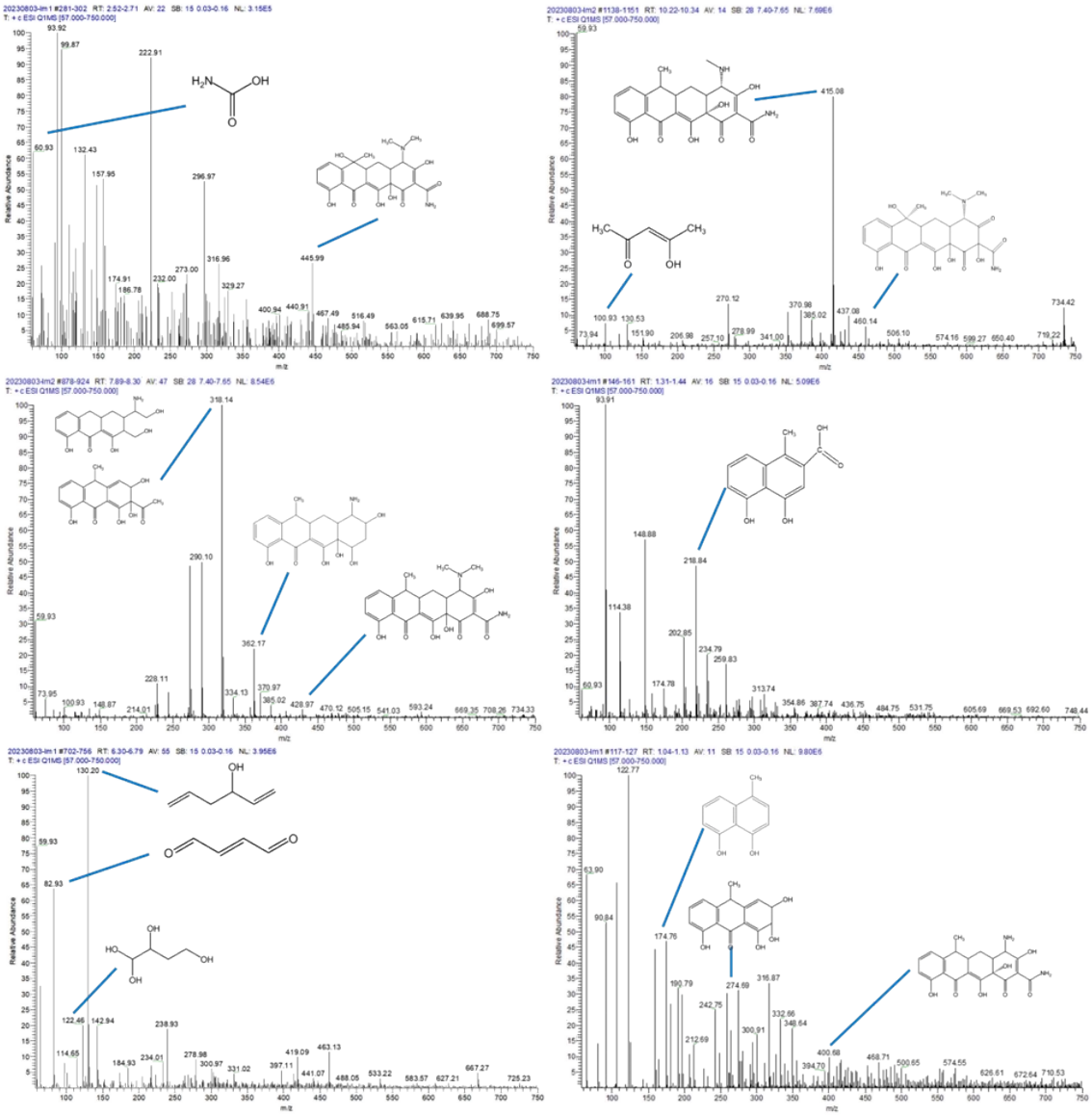

Fig. S10. LC−MS analysis of 10CN-MMT/PMS/TC in 15 and 60 min.

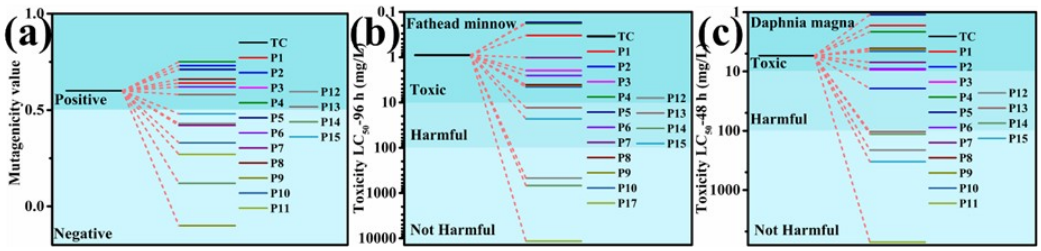

Fig. S11. Mutagenicity value (a), acute toxicity LC50 of fathead minnow (b), and acute toxicity LC50 of daphnia magna (c) of TC and its intermediate products.

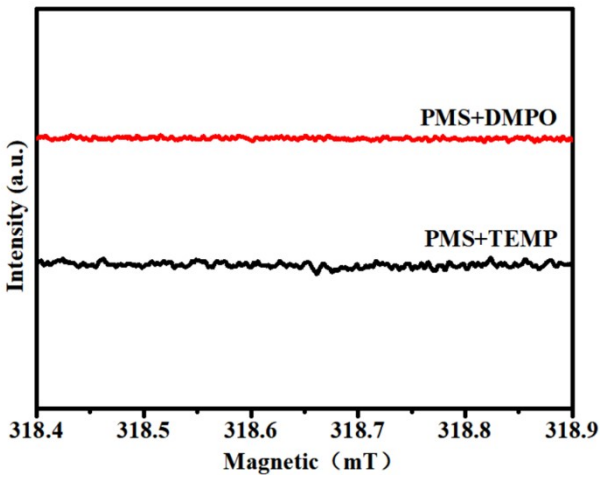

Fig. S12. ESR spectra of pure PMS in aqueous solution.

References

1 Y, Zhang, T, Wang, X, Zhang, Y, Sun, G. Fan, G. Song, and B. Chai, Appl. Surf. Sci., 2024, **647**, 158965.

2 M. Cheng, R. Ma, G. Chai, Y. Chen, L. Bai, D. Wang, J. Qian, and G. Chen, Chem. Eng. J., 2023, **453**, 39810.

3 X. Li, Z. Ye, S. Xie, H. Li, Y. Lv, Y. Wang, Y. Wang, and C. Lin, J. Environ. Chem. Eng., 2022, **10**, 108264.

4 X. Liu, J. Zhou, and D. Liu, J. Environ. Chem. Eng., 2022, **10**, 107833.

5 S. Kumar, C. Tewari, N. G. Sahoo, and L. Philip, J. Hazard. Mater. 2022, **435**, 128956.

6 G. Liu, C. Li, B. A. Stewart, L. Liu, M. Zhang, M. Yang, and K. Lin, Chem. Eng. J., 2020, **399**, 125722.

7 J. Yang, X. He, J. Dai, Y. Chen, Y. Li, and X, Hu, Environ. Res. 2021, **194**, 110496.

8 S. Cai, X. Zuo, H. Zhao, S. Yang, R. Chen, L. Chen, R. Zhang, D. Ding, and T. Cai,

J. Mater. Chem. A, 2022, **10**, 9171.

9 X. Zhang, R. Zhao, N. Zhang, Y. Su, Z. Liu, R. Gao, C. Du, Appl. Catal. B, 2020, **263**, 118316.

10 S. Wang, and J. Wang, Chem. Eng. J., 2019, **356**, 350-358.

11 C. Rao, L. Zhou, Y. Pan, C. Lu, X. Qin, H. Sakiyama, M. Muddassir, and J. Liu, J. Alloys Compd., 2022, **897**, 163178.

12 X. Zhang, M. Li, Y. Su, and C. Du, Appl Clay Sci, 2021, **211**, 106208.